

Multipeak characteristics of field emission energy distribution from semiconductorsR. Z. Wang,^{1,2} X. M. Ding,¹ K. Xue,⁴ B. L. Zhao,¹ H. Yan,³ and X. Y. Hou^{1,*}¹*Surface Physics Laboratory (National Key Laboratory), Fudan University, Shanghai 200433, China*²*College of Science, Zhejiang University of Science, Hangzhou 310018, China*³*Quantum Material Laboratory, Beijing University of Technology, Beijing 100022, China*⁴*Department of Electronic Engineering, The Chinese University of Hong Kong, Hong Kong, China*

(Received 10 June 2004; published 5 November 2004)

Multipeak characteristics of field emission energy distribution (FEED) from semiconductor films has been investigated theoretically. It is shown that for wide bandgap semiconductors with low or negative electron affinity, the appearance of FEED multipeaks is inevitable when a high electric field is applied, and the extra peaks will become pronounced while the peak positions shift toward the lower energy side with increasing field, which agrees well with experimental observations. It is also found that the number, strength, and position of FEED peaks are strongly dependent on factors such as field intensity, electron affinity, and doping levels. Resonant electron tunneling is suggested as an appropriate model to describe the FEED multipeak characteristics observed.

DOI: 10.1103/PhysRevB.70.195305

PACS number(s): 79.70.+q, 73.40.Gk, 73.20.At, 02.60.Cb

I. INTRODUCTION

Since Henderson and Dahlstrom¹ first investigated the field emission energy distribution (FEED) of tungsten using a retarding potential analyzer, the analysis of FEEDs has become an important approach to address the origination of field emission. Metals were studied intensively both experimentally and theoretically due to their simplicity;²⁻⁵ a single FEED peak is usually observed. In 1966, Swanson and Crouser⁴ observed for the first time an anomalous total energy distribution (TED) with a shoulder from a tungsten field emitter; in 1992, Binh *et al.*⁶ observed clearly well-separated peaks of FEED from tungsten nanoprotusion tips. For FEEDs of semiconductors, Stratton⁷ presented a detailed theory in 1964; however, there were few experimental reports of FEED from semiconductor films until the 1990's. Recently, due to outstanding field emission properties of wide bandgap semiconductor (WBGs) films,⁸ FEEDs from semiconductors have attracted much attention.⁹⁻¹⁵ Thin films of WBGs's such as diamond^{9,13-15} and cubic boron nitride (c-BN)¹²⁻¹⁴ have been intensively studied. The FEEDs of these materials generally showed the existence of a single FEED peak. Very recently, an additional FEED peak in higher field intensity was reported for WBGs's: Chen *et al.*¹⁰ observed repeatedly the two-peak feature of the FEED from amorphous carbon nitride films, and Collazo *et al.*¹¹ found a two-component energy distribution characteristic of field emission from AlN films under higher fields. In fact, a little earlier, Gröning *et al.*⁹ studied the energy distribution of the electrons emitting from nitrogen-containing diamondlike carbons and a small second FEED peak was also observed, but they neglected this small FEED peak and even did not mention it in their work. These experimental results showed FEED multipeak characteristics from semiconductors in high fields should be intrinsic. Nevertheless, to the best of our knowledge, no thorough theoretical investigations have been

reported on the FEED multipeak effect from semiconductors. For the FEED multipeak behavior of metal, only Nagy and Cutler⁵ calculated the anomalous TED⁴ from tungsten based on Stratton's theory.⁷ Because of oversimplification of the band structure model used in their calculation, the results exhibited observable discrepancies in both the shape and the position of the second peak from those experimentally observed. Binh *et al.*⁶ pointed out previously that the simplified band structure model could not even explain the experimentally observed enhancement of the first peak of FEED with increasing field. Further theoretical investigation on the phenomena is obviously needed.

In this paper, by taking into consideration the overall field effect on the band structure and on the surface potential barrier, we put forward a resonant tunneling model to describe the multipeak characteristics of FEEDs from semiconductors. Our calculations show that a distinct two-peak characteristic of FEEDs is inevitable with increasing field intensity, in good agreement with experimental results.^{10,11} Moreover, the calculated results show that, besides the field intensity, a low or negative electron affinity is also a key factor to the appearance of the FEED multipeak characteristics. Also taken into consideration in our calculations is the effect of doping on the FEED characteristics, and the results show that heavy doping will lead to the multipeak characteristics; even more than two peaks may appear in the FEED of a very heavily doped semiconductor.

II. THEORETICAL MODEL

To emphasize the physics behind and to simplify the numerical calculation process, we focus on not the total energy distribution, but on the normal energy distribution and separate the supply functions and the transmission coefficient.

The field emission in a semiconductor can be expressed as¹⁶

$$J = \frac{4\pi q m_i k_B T}{h^3} \int T(E_x) \ln[1 + e^{-(E_x - E_F)/k_B T}] dE_x = \int J(E_x) dE_x, \quad (1)$$

where q is the unit charge, m_i is the electron transverse mass, k_B is Boltzmann's constant, $E_x = P_x^2/2m$ is the normal energy, T the temperature, h is Plank's constant, and E_F is the Fermi energy. $J(E_x)$ is the expression of normal-energy distribution written as

$$J(E_x) = \frac{4\pi q m_i k_B T}{h^3} \cdot \ln[1 + e^{-(E_x - E_F)/k_B T}] \cdot T(E_x). \quad (2)$$

Equation (2) is made up of the transmission coefficient $T(E_x)$ and the supply function. Transmission coefficient $T(E_x)$ can be calculated by the transfer matrix (TM) method^{17,18} based on the analytical solution of Schrödinger equation with a linear potential, and the solution can be expressed as a linear combination of the Airy function or other wave functions. In this method, an arbitrary potential barrier can be divided into square segments that can be treated as linear barriers. Compared with the Wentzel-Kramers-Brillouin (WKB) method, the TM method is based on an accurate solution of Schrödinger equation, so that the results are much closer to the realistic depiction of the tunneling process during field emission.

In our calculations, m_i and E_F are treated as experimental fitting parameters, set by the specific semiconductor band structure. Thus, the detailed band structures can be simplified as only the density of occupied states needs to be considered in computing the supply function. However, band bending in high fields should be considered, because the maximum value of the band bending, which is almost in linear proportion to the bandgap of WBGs's, may be as high as several electron volts.¹⁹ One should also consider that carriers in semiconductors may form a space charge region under high fields, which can be best described by Poisson's equation as

$$\frac{d^2 \phi(x)}{dx^2} = \frac{e}{\epsilon \epsilon_0} \rho(x). \quad (3)$$

Here, $\phi(x)$ and $\rho(x)$ denote, respectively, the potential energy and the total volume charge density at the place with distance x from the semiconductor-vacuum interface, and ϵ_0 and ϵ are the vacuum permittivity and the semiconductor dielectric constant, respectively. Assuming $\varphi = \phi/kT$, $\rho(\varphi)$ can be given as

$$\rho(\varphi) = e[n_p(\varphi) - n_c(\varphi) - (N_a^- - N_d^+)], \quad (4)$$

where $n_c(\varphi)$ is the electron concentration in the conduction band, $n_p(\varphi)$ is the hole concentration in the valence band, and N_a^- and N_d^+ are the ionized acceptor and donor concentrations, respectively. When an external field is applied, by assuming constant density of states model, $n_c(\varphi)$ and $n_p(\varphi)$ can be obtained by

$$n_c(\varphi) = 2 \frac{(2\pi m_n^* kT)^{3/2}}{h^3} \exp\left(-\frac{E_c - E_F}{kT} - \varphi\right), \quad (5)$$

$$n_p(\varphi) = 2 \frac{(2\pi m_p^* kT)^{3/2}}{h^3} \exp\left(\frac{E_v - E_F}{kT} + \varphi\right), \quad (6)$$

$$N_a^- - N_d^+ \cong 2n_i \sinh(\varphi_B), \quad \varphi_B = \frac{E_F - E_{Fi}}{kT}, \quad (7)$$

where k is Boltzmann's constant, h is Planck's constant, m_n^* and m_p^* are, respectively, the effective masses of electron and hole, E_F and E_{Fi} are, respectively, Fermi and quasi-Fermi energies, n_i is the intrinsic carrier concentration, E_c is the minimum of the conduction band, and E_v is the maximum of the valence band. The intrinsic carrier concentration is given by

$$n_i = 2 \left(\frac{2\pi kT}{h^2}\right)^{3/2} (m_n^* m_p^*)^{3/4} e^{-E_g/2kT}, \quad (8)$$

where E_g is the bandgap ($E_g = E_c - E_v$). Combining Eqs. (4)–(8) with (3), one can obtain

$$\int_0^{-x_1} \frac{dx}{\delta} = \int_{\varphi_s}^{\varphi} \frac{d\varphi}{f(\varphi, \varphi_B)}. \quad (9)$$

Here, $\varphi_s = (\phi_s - \phi_B)/kT$, ϕ_s is the band bending at the interface ($x=0$), $\delta = (\epsilon \epsilon_0 kT / 2n_i e^2)^{1/2}$ is known as the Debye screening length, and $f(\varphi, \varphi_B)$ can be expressed by

$$\begin{aligned} f(\varphi, \varphi_B) &= \frac{\delta d\varphi}{dx} \Big|_{\varphi} = \left(\int_{\varphi_B}^{\varphi} \left\{ \left[\left(\frac{m_p^*}{m_n^*} \right)^{3/4} \exp\left(\frac{E_v - E_F}{kT} + \varphi\right) \right. \right. \right. \\ &\quad \left. \left. \left. - \left(\frac{m_n^*}{m_p^*} \right)^{3/4} \exp\left(-\frac{E_c - E_F}{kT} - \varphi\right) \right] \right. \right. \\ &\quad \left. \left. - 2 \sinh(\varphi_B) \right\} d\varphi \right)^{1/2} \\ &= \{a[\exp(\varphi) - \exp(\varphi_B)] - b[\exp(-\varphi_B) \\ &\quad - \exp(-\varphi)] - 2 \sinh(\varphi_B)(\varphi - \varphi_B)\}^{1/2}, \end{aligned} \quad (10)$$

where

$$a = \left(\frac{m_p^*}{m_n^*}\right)^{3/4} \exp\left(\frac{E_v - E_F}{kT}\right), \quad (11)$$

$$b = \left(\frac{m_n^*}{m_p^*}\right)^{3/4} \exp\left(-\frac{E_c - E_F}{kT}\right). \quad (12)$$

Thus, the potential shape in the space charge region can be derived numerically from Eq. (9) and the interface electric field E_S can be obtained from

$$E_S = \frac{d\phi}{edx} = \frac{kT}{e\delta} \left. \frac{\delta d\phi}{dx} \right|_{\varphi_S} = \frac{kT}{e\delta} f(\varphi_S, \varphi_B). \quad (13)$$

Compared with Tsong's model,²⁰ the function $f(\varphi_S, \varphi_B)$ is calculated in a much simpler way in that only the basic data of m_n^* and m_p^* are needed, which can easily be obtained for both intrinsic and doped semiconductors. In addition, the band bending can be easily obtained from $f(\varphi_S, \varphi_B)$.

In the TM method for computing $T(E_x)$, potential barrier shape is a key parameter affecting the transmission coefficient dramatically, so we considered a more complicated and realistic image potential:²¹

$$V_S(z) = \frac{q^2}{16\pi\epsilon_S\epsilon_0} \sum_{n=0}^{\infty} (\beta\beta')^n \left[\frac{\beta}{ns-z} - \frac{\beta'}{(n+1)s-z} \right], \quad (14)$$

where s is the vacuum gap, q is unit charge, ϵ_S is dielectric permittivity of the semiconductor, ϵ_0 is the permittivity of vacuum, $\beta = (\epsilon_S - \epsilon_0)/(\epsilon_S + \epsilon_0)$, and $\beta' = 1$ for a metal-vacuum-semiconductor junction. We base our calculation on the sandwiched model with a vacuum between the semiconductor cathode and the metal anode. However, since the image potential in the form of Eq. (14) does not include the field penetration, it is not proper concerning the interfaces, where $V_S(z)$ tends to be negative infinite. To be more realistic, the image potential shifting should be considered.²² Thus, we re-form Eq. (14) by adding the shift lengths r_1 and r_2 into the semiconductor and the metal, respectively. Equation (14) can then be rewritten as

$$V_S(z) = \frac{q^2}{16\pi\epsilon_S\epsilon_0} \sum_{n=0}^{\infty} (\beta\beta')^{2n+1} \left[\frac{\beta}{(2n+1)s-z+r_1} - \frac{\beta'}{(2n+2)s-z-r_2} \right] + \frac{q^2}{16\pi\epsilon_S\epsilon_0} \sum_{n=0}^{\infty} (\beta\beta')^{2n} \left[\frac{\beta}{2ns-z-r_1} - \frac{\beta'}{(2n+1)s-z+r_2} \right]. \quad (15)$$

Since the shift length decreases with increasing surface charge density²² and the surface charge density in the metal is larger than that in the semiconductor, we assume $r_1 = 1.2$ a.u. and $r_2 = 1.6$ a.u. based on reported data (See Ref. 22, 1 a.u. = 0.529 Å).

Figure 1 is the potential distribution of c-BN with the band bending and the effective image potential taken into consideration, where E_g and electron affinity are chosen to be 6.5 and -0.3 eV, respectively.¹⁹ Other parameters are the same as in our previous work.¹⁹

III. RESULTS AND DISCUSSION

As an example, we present here the calculated FEED of c-BN. The reason for selecting c-BN lies in its superior properties as an excellent field emitter,²³ such as chemical and

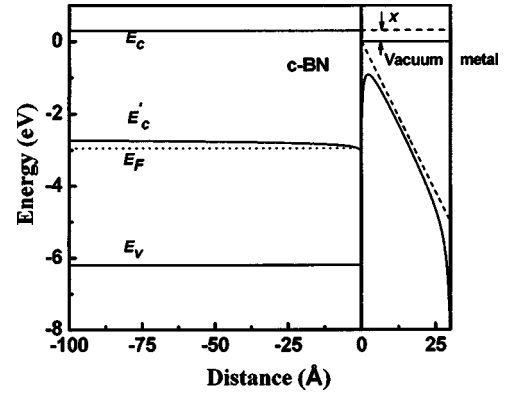


FIG. 1. Energy band diagram of the c-BN/vacuum/metal structure with a voltage of 5 V applied between c-BN and metal, where E'_c and E_c are the conduction band minimum without and with the field applied, respectively, and E_v is the valence band maximum.

thermal stability, and its behavior as a typical WBGs. In the reported experimental results of semiconductors,¹⁰⁻¹² only WBGs's show the multipeak behavior in FEED.

A. FEED versus field strength

Figure 2 shows the multipeak FEED calculated for c-BN. In the calculations, we kept a constant distance of 3 nm between the anode and the cathode and varied the applied voltage to study the dependence of FEED on the electric field. The adoption of a constant cathode-anode distance was for ease in modeling the system. FEEDs measured from a real sample configuration, in which the vacuum gap could be much larger than 3 nm, may deviate from those shown in the figure to some extent. However, the main features, such as the number of the peaks, of the calculated and measured curves should principally the same if the same field intensity is kept in the two cases. In our calculations, the field intensity varied from 0.67 to 2.0 V/nm, which matches the real systems well: the field intensity in a real system may even be higher than 2 V/nm when the geometric electric field enhancement is taken into consideration.

One may notice in the figure that the multipeak behavior becomes more obvious in increased fields, which is in good agreement with the experimental results.^{10,12} With a low field applied, only one peak appears as shown in the inset of Fig.

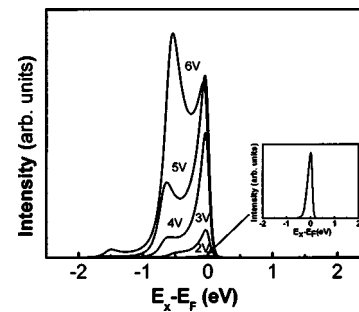


FIG. 2. FEEDs of c-BN at different applied voltages, with the vacuum gap kept constant at 3 nm.

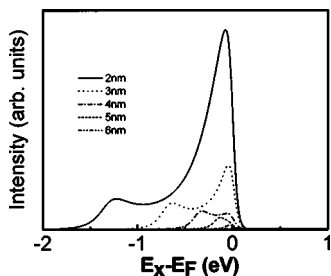


FIG. 3. FEEDs of c-BN at different vacuum gaps, with the applied voltage kept constant at 5 V.

2; when in increased fields, a second peak becomes pronounced, with its position shifting toward the lower energy side. Such a behavior coincides with what was previously found for metals. Binh *et al.*²⁴ observed experimentally that the well-separated peaks of FEED occurred only in the case of nanoprotrusion tips with localizing enough high field intensity. They showed an evolution of the TED's versus protrusion height on the same base tip. As the height of the protrusion increased, i.e., the localized field over the protrusion apex increased, emergence of the second FEED peak became pronounced, same as our calculated results for semiconductors shown in Fig. 2.

We have also kept the voltage constant and changed the distance between the anode and the cathode to vary the field intensity, and got a similar behavior of FEED, as shown in Fig. 3. Based on these observations, we propose that the field intensity is a key factor for the multipeak characteristic of FEED.

B. Negative electron affinity (NEA) effects

By maintaining other parameters constant and changing only the electron affinity, we studied NEA's effects on FEED of c-BN. In Fig. 4, with the electron affinity decreased, a second peak of FEED appears and gets stronger. It is obvious that the negative electron affinity is also an important factor to affect the multipeak behavior. Experimental results also proved this, for multipeak characteristic of FEED could be found in some WBGs's with NEA.¹⁰⁻¹²

C. Doping effects

In addition to the field intensity itself, doping may affect field emission properties for some semiconductors. To get a

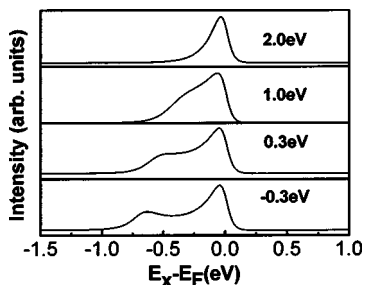


FIG. 4. FEEDs of c-BN at different electron affinities, with the applied voltage of 5 V and the vacuum gap of 3 nm.

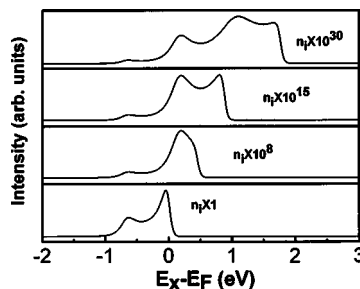


FIG. 5. FEEDs of c-BN at different *n*-doping concentrations, with the applied voltage of 5 V and the vacuum gap of 3 nm.

more completed understanding of multipeak behavior in FEED, it should be interesting to examine the effect of doping on multi-peaks of FEED. In Fig. 5, we show the calculated FEED of c-BN for different *n* doping. The results show that the number of the peaks of FEED increases when the doping concentration is increased. Unlike previous work, our study shows that there may be more than two peaks of FEED in the case of heavy *n* doping. Further experimental support is obviously needed.

D. Mechanism of FEED multipeak formation

In previous theoretical researches on the FEEDs of semiconductors,^{7,25} the phenomena of the multipeak FEED were not observed theoretically. This might be due to two reasons: first, the transmission coefficient was probably obtained with the WKB methods,⁷ which made the resonance of the transmission coefficient disappear inadequately;²⁶ second, the applied fields might not be high enough or the electron affinity might not be low enough.²⁵

In order to understand the physics of the multipeak characteristic of FEED, one should focus on the process of electron tunneling in field emission from semiconductors. In our calculations, all the effects intrinsic to the band structure of the semiconductor were ignored, so the FEED calculated could only be attributed to electrons tunneling through the surface potential barrier under high fields. In other words, the multipeak characteristic of the FEED may root in resonant tunneling through a single-barrier (see Fig. 1). It may originate from interference of incident and reflected electron waves at the surface potential barrier interface.²⁶ Plotting the field emission current making up of the supply function and

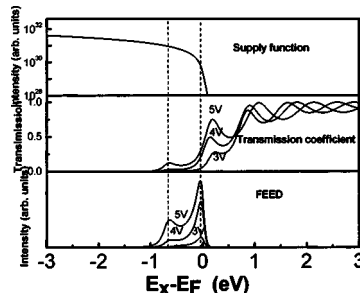


FIG. 6. Illustration of the FEED multipeak characteristics by separating Eq. (2).

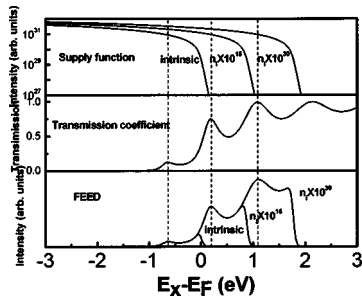


FIG. 7. Illustration of the FEED multippeak characteristics with different n -doping concentration.

the transmission coefficient based on Eq. (2), we can understand clearly the substance of the multippeak characteristic of the FEED as shown in Fig. 6. Due to great contribution of the supply function, there is a resonant peak of transmission on the low energy side; a second peak is formed in the region where the supply function exaggeratedly decreases. The resonant peak of transmission disappears for negligible supply function contributions on the high energy side. As the field intensity is changed, it can be seen easily in Fig. 6 that the magnitude of the second peak of the FEED rests with the strength of the resonant peak of transmission coefficient on the low energy side. This means that the appearance of the multippeak characteristic of the FEED may originate from resonant tunneling through the surface potential barrier. On the other hand, the oscillatory behavior of the tunneling coefficient is also presumed to be due to resonance through the virtual states above the barrier;²⁷ it also indicated that there may be multippeak characteristics of the FEED in the semiconductors with NEA.

Figure 7 shows the multippeak characteristic of FEEDs with different n doping levels. As the n -doping concentration increases, the supply function shifts toward the high energy side, which holds the resonant peaks of the transmission coefficient. This will lead to an increase in the number of peaks.

The multippeak characteristics of the FEEDs from semiconductors were observed repeatedly in some recent

experiments.^{10–12} However, only a single FEED peak was observed in the previous theory.^{7,25} To explain this phenomenon, Chen *et al.*¹⁰ assumed that the small peaks might originate from the interband states due to defects or doping in semiconductor films, while Collazo *et al.*¹¹ thought that the intervalley scattering was evidenced by a multicomponent energy distribution featuring a second peak at the energy position of the first satellite valley under high fields. However, neither interband states nor intervalley scattering is taken into consideration in our model, but the multippeak characteristics of FEEDs in semiconductors can be still obtained. Based on our results, the multippeaks of the FEEDs of semiconductors may originate from electron resonant tunneling through the surface potential barrier under the high field intensity.

IV. CONCLUSIONS

We adopt a resonant tunneling model to theoretically study multippeak characteristics of the FEEDs of semiconductors. It is shown that electric field combined with NEA and doping level have strong effects on the property of multippeak behavior. Upon increasing the applied field, the second peak will appear and shift to the lower energy side, while a decrease in NEA or an increase in doping may lead to similar effects.

From our calculation, the origin of multippeaks may come from electron resonant tunneling through the surface potential barrier, since electric field, electron affinity, and doping level determine the potential barrier, and these factors have a strong effect on the resonant tunneling process, leading to the FEED multippeak characteristics.

ACKNOWLEDGMENTS

This work is supported by the CNKBRSF, the National Natural Foundation of China under Grant No. 10321003, and the Science and Technology Commission of Shanghai Municipality.

*Author to whom correspondence should be addressed; electronic mail: xyhou@fudan.edu.cn

¹J. E. Henderson and R. K. Dahlstrom, Phys. Rev. **55**, 473 (1939).

²J. W. Gadzuk and E. W. Plummer, Rev. Mod. Phys. **45**, 487 (1973).

³R. Fisher, Phys. Status Solidi **2**, 1088 (1962).

⁴L. W. Swanson and L. C. Crouser, Phys. Rev. Lett. **16**, 389 (1966).

⁵D. Nagy and P. H. Cutler, Phys. Rev. **186**, 651 (1969).

⁶V. T. Binh, S. T. Purcell, N. Garcia, and J. Doglioni, Phys. Rev. Lett. **69**, 2527 (1992).

⁷R. Stratton, Phys. Rev. **135**, A794 (1964).

⁸M. W. Geis, N. N. Efremow, K. E. Krohn, J. C. Twichell, T. M. Lyszczarz, R. Kallish, J. A. Greer, and M. D. Tabat, Nature (London) **393**, 431 (1998).

⁹O. Gröning, O. M. Küttel, P. Gröning, and L. Schlapbach, Appl. Phys. Lett. **71**, 2253 (1997).

¹⁰J. Chen, N. Y. Huang, X. W. Liu, S. Z. Deng, and N. S. Xu, J. Vac. Sci. Technol. B **21**, 567 (2003).

¹¹R. Collazo, R. Schlessler, A. Roskowski, P. Miraglia, R. F. Davis, and Z. Sitar, J. Appl. Phys. **93**, 2765 (2003).

¹²B. L. McCarson, R. Schlessler, and Z. Sitar, J. Appl. Phys. **84**, 3382 (1998).

¹³R. Schlessler, M. T. McClure, and Z. Sitar, J. Vac. Sci. Technol. B **16**, 689 (1998).

¹⁴R. Schlessler, M. T. McClure, B. L. McCarson, and Z. Sitar, J. Appl. Phys. **82**, 5763 (1997).

¹⁵R. Schlessler, M. T. McClure, W. B. Choi, J. J. Hren, and Z. Sitar, Appl. Phys. Lett. **70**, 1596 (1997).

¹⁶R. Water and B. V. Zeghbroeck, Appl. Phys. Lett. **75**, 2410 (1999).

- ¹⁷R. Z. Wang and X. H. Yan, *Chin. Phys. Lett.* **17**, 598 (2000).
- ¹⁸J. Q. You, L. D. Zhang, and P. K. Ghosh, *Phys. Rev. B* **52**, 17 243 (1995).
- ¹⁹R. Z. Wang, B. Wang, H. Wang, H. Zhou, A. P. Huang, M. K. Zhu, H. Yan, and X. H. Yan, *Appl. Phys. Lett.* **81**, 2782 (2002).
- ²⁰T. T. Tsong, *Surf. Sci.* **81**, 28 (1979).
- ²¹Z. H. Huang, M. Weimer, and R. E. Allen, *Phys. Rev. B* **48**, 15 068 (1993).
- ²²N. D. Lang and W. Kohn, *Phys. Rev. B* **7**, 3541 (1973).
- ²³R. W. Pryor, *Diamond for Electronic Applications*, MRS Symposia Proceedings No. 416 (Materials Research Society, Pittsburgh, 1996), p. 425.
- ²⁴V. T. Binh, S. T. Purcell, and N. Garcia, *Phys. Rev. Lett.* **70**, 2504 (1993).
- ²⁵M. S. Chung, N. M. Miskovsky, P. H. Cutler, and N. Kumar, *Appl. Phys. Lett.* **76**, 1143 (2000).
- ²⁶K. H. Gundlach, *Solid-State Electron.* **9**, 949 (1966).
- ²⁷T. W. Hickmott, P. M. Solomon, R. Fischer, and H. Morkoc, *Appl. Phys. Lett.* **44**, 90 (1984).